Configuration mixing of angular-momentum and particle-number projected triaxial Hartree-Fock-Bogoliubov states using the Skyrme energy density functional

Michael Bender[1,2,3,4,5,6,7] and Paul-Henri Heenen[1]

[1]*Service de Physique Nucléaire Théorique, Université Libre de Bruxelles, C.P. 229, B-1050 Bruxelles, Belgium*
[2]*Institute for Nuclear Theory, University of Washington, Box 351550, Seattle, Washington 98195, USA*
[3]*Physics Division, Argonne National Laboratory, 9700 S. Cass Avenue, Argonne, Illinois 60439, USA*
[4]*National Superconducting Cyclotron Laboratory, Michigan State University, 1 Cyclotron, East Lansing, Michigan 48824, USA*
[5]*DAPNIA/SPhN, CEA Saclay, F-91191 Gif sur Yvette Cedex, France*
[6]*Université Bordeaux, Centre d'Etudes Nucléaires de Bordeaux Gradignan, UMR5797, F-33175 Gradignan, France*
[7]*CNRS/IN2P3, Centre d'Etudes Nucléaires de Bordeaux Gradignan, UMR5797, F-33175 Gradignan, France*

We present a method based on mean-field states generated by triaxial quadrupole constraints that are projected on particle number and angular momentum and mixed by the generator coordinate method on the quadrupole moment. This method is equivalent to a seven-dimensional GCM calculation, mixing all five degrees of freedom of the quadrupole operator and the gauge angles for protons and neutrons. A first application to ^{24}Mg permits a detailed analysis of the effects of triaxial deformations and of K mixing.

I. INTRODUCTION

Methods based on the self-consistent mean-field approach [1] are up to now the only microscopic tools that can be applied to all nuclei including the heaviest ones. However, mean-field methods have several limitations, and the method that we present here is part of an attempt to eliminate two of the most penalizing presented in a series of papers. The first limitation is due to the determination of a wave function in an intrinsic frame of reference. Although the symmetry-breaking mean-field approach is a very efficient and transparent way to grasp the effect of correlations associated with collective modes in the limit of strong correlations [2–5], the absence of good quantum numbers and the corresponding selection rules does not allow direct determination of the electromagnetic transition probabilities. Instead, approximations have to derived based on the collective model and these cannot cover all possible cases as they are well justified only in the limit of large deformation. The second limitation concerns nuclei for which a mean-field description through a single configuration breaks down because several configurations with different shell structure are close in energy without being separated by a large potential barrier. Methods to overcome these two problems have been proposed in the past, but it is only in the last ten years that sufficient computational resources have become available to construct and apply methods based on realistic effective energy density functionals aiming at eliminating both of these limitations.

Angular momentum projection [5–7] is the key tool to transform the mean-field wave function from the intrinsic to the laboratory frame of reference. There is no ambiguity in determining directly electromagnetic transition probabilities when working in the laboratory system. However, without the simplifying assumption of axial states, the restoration of rotational symmetry requires that rotations about three Euler angles be considered. So far, for mean-field states with triaxial quadrupolar deformations, this has been mostly done in the context of phenomenological models by using small shell model spaces and often schematic interactions [8–13]. In the context of energy density functional methods, projection on angular momentum of mean-field states with triaxial quadrupolar deformations has been performed at the Hartree-Fock level by using a simplified Skyrme interaction in Ref. [14] and very recently with a full Skyrme energy functional in Ref. [15]. Cranked wave functions have been projected in both cases to approximate a variation after projection on the angular momentum [16–18], but pairing correlations were not included.

To solve the problem of energy surfaces that are soft with respect to a collective degree of freedom, one has to introduce fluctuations in this collective degree of freedom into the ground-state wave function using the generator coordinate method (GCM) [5–7,19]. Again, many studies used small shell model spaces and schematic interactions, but there is also a quite a large body of work starting from mean-field methods based on effective interactions in the full model space of occupied single-particle states and with inclusion of pairing correlations. There have been several applications [20–22] that deal with the intrinsic quadrupole mode including triaxial deformations, which is in most cases the dominant low-lying collective excitation mode in nuclei. There also have been studies of octupole modes [23–25] and their coupling to the quadrupole mode [26,27], as well as investigations of fluctuations in pairing degrees of freedom [28–30]. All the studies mentioned so far have in common the fact that simultaneous symmetry restoration, if performed at all, is limited to numerically inexpensive modes, such as particle number or parity, whereas angular momentum is not restored.

A simultaneous treatment of angular momentum projection and of fluctuations with respect to triaxial quadrupole deformation requires that five degrees of freedom be considered. The most transparent representation consists of three Euler angles defining the relative orientation of the intrinsic major axis frame in the laboratory frame and two independent degrees of

freedom characterizing the intrinsic deformation (e.g., through the coordinates β and γ introduced by Å. Bohr). In the context of the GCM, however, this has so far only been done in highly schematic models, by using either a single-j shell [31] or a very small shell model space and a schematic interaction [32,33].

A first step toward the simultaneous treatment of these five degrees of freedom has been carried out recently with the GCM mixing of angular-momentum projected quadrupole-deformed axial mean-field states. This scheme is nowadays routinely applied by several groups, using Skyrme energy density functionals [34–36], the density-dependent Gogny force [37–39], or a relativistic point-coupling model [40,41]. In all of those cases, intrinsic triaxiality is neglected and two of the three Euler angles can be treated analytically.

All the studies mentioned so far that consider angular momentum projection have in common the fact that this operation is performed after variation. This has several drawbacks [5], in particular when working with time-reversal invariant mean-field states. The alternative, variation after projection, is computationally very demanding. The only standard method where variation after angular-momentum projection is considered (together with restoration of N, Z, and parity) is the VAMPIR/MONSTER approach [42,43], which is confined to a very small shell model space and a shell model effective Hamiltonian. In this framework, the intrinsic dynamics is not described in terms of deformation degrees of freedom, but rather in terms of quasiparticle excitations.

An approximate scheme to describe five-dimensional quadrupole dynamics in a fully microscopic framework has been set up long ago. The idea is to construct the input of the Bohr Hamiltonian microscopically [5,20,44]. This is an approximation to the full five-dimensional GCM as it replaces the nonlocal kernels entering the Hill-Wheeler-Griffin equation for nonorthogonal weight functions by local potentials and mass parameters in a collective Schrödinger equation for orthogonal collective wave functions, but it also allows one to incorporate improved moments of inertia at a moderate cost. This approach has routinely been used for a long time in the framework of the density-dependent Gogny force [45,46], and it has also been recently set up for Skyrme interactions [47].

In this paper we present a first step toward a microscopic treatment of triaxial quadrupole dynamics and of angular momentum projection in the context of nuclear energy density functional methods using the full space of occupied single-particle states. The method employed generalizes that described in Refs. [34–36] by allowing for the breaking of axial symmetry of the mean-field wave functions.

II. THE METHOD

For a given nucleus, the calculations are performed in three steps. First, a nonorthogonal basis of self-consistent mean-field states is generated with constrained Hartree-Fock-Bogoliubov (HFB) calculations. Second, angular-momentum and particle-number projected matrix elements between all mean-field states are calculated. Third, these matrix elements are used in a configuration-mixing calculation to determine the correlated

ground state, the spectrum of excited states, and the transition moments

The only inputs to the calculation are the proton and neutron number and the parameters of a universal energy functional. The latter are taken from the literature and obtained from a global fit to nuclear properties aiming at the description of the entire chart of nuclei, without local fine tuning. One consistency requirement of our method is that the same effective interaction is used to generate the mean-field states and to calculate the configuration mixing. We chose a Skyrme energy functional supplemented by the Coulomb interaction in the mean-field channel, together with a zero-range, density-dependent functional in the pairing channel.

We will give here, and in the Appendix, only a sketch of the ingredients of the method. We postpone a detailed description to a future paper on the generalization of the code to time-reversal invariance breaking triaxial states.

A. The mean-field basis

The HFB equations are solved self-consistently with the two-basis method of Ref. [48]. The quadrupole moment is constrained through two coordinates q_1 and q_2, which are related to the usual mass quadrupole deformations β and γ of the Bohr Hamiltonian through the relations [49]

$$q_1 = Q_0 \cos(\gamma) - \frac{1}{\sqrt{3}} Q_0 \sin(\gamma), \tag{1}$$

$$q_2 = \frac{2}{\sqrt{3}} Q_0 \sin(\gamma), \tag{2}$$

with

$$\beta_2 = \sqrt{\frac{5}{16\pi}} \frac{4\pi Q_0}{3 R^2 A}, \tag{3}$$

where $R = 1.2 A^{1/3}$ fm. A mesh of positive values for q_1 and q_2 covers the entire first sextant of the β-γ plane. The mean-field equations are solved on a three-dimensional mesh [49], with the total nuclear density imposed to be symmetric with respect to the three planes. Thus, all odd-l moments of the density identically vanish whereas the even moments, which are not constrained, are fully taken into account and take the values that minimize the energy. All the wave functions that we consider are, therefore, restricted to have positive parity.

For the results described in the following, the mean-field wave functions are required to be time-reversal invariant, such that the collective coordinates can be limited to one sextant of the β-γ plane. The five other sextants correspond to one or several permutations of the principle axes of inertia. After projection and configuration mixing, all of them are equivalent, although intermediate (nonobservable) quantities might differ. This equivalence will be used as a test of the numerical implementation of our method of Sec. III.

B. Projection

Restoring symmetries allows one to extract states with good quantum numbers from the mean-field states and provides a

clean framework to use selection rules for electromagnetic transitions. Eigenstates of the particle-number operator are obtained in the same way as previously [35,36]. From a technical point of view, it is crucial to restore this symmetry when mixing wave functions that are not eigenstates of the particle-number operators. Since those wave functions have only the right mean particle number, their transition matrix elements will contain nondiagonal contributions in the number of particles. One can estimate easily the error that this symmetry breaking brings to energies. The binding energy per nucleon of most nuclei is between 7 and 8 MeV/u and a deviation of the particle number of a mixed state as small as 0.1 nucleons would affect its energy by several hundreds of keV. Particle-number projection removes this ambiguity [22]. A technically simpler approximate method would be to introduce a constraint on the average value of the particle number N_0 of the mixed states in the Hill-Wheeler-Griffin equation [20,38], but since the same value for this constraint has to be used for all the eigenstates to maintain their orthogonality, the error on the mean number of particles will vary from one state to another. We always project on the proton and neutron numbers imposed on the mean-field wave functions by Lagrange multipliers in the mean-field equations. We, therefore, drop any reference to particle numbers for the sake of simple notation.

Angular momentum projection is significantly more complicated when triaxial mean-field states instead of axial ones are considered. Eigenstates of the total angular momentum operator in the laboratory frame, $\hat{J}^2$, and its projection on the z axis, $\hat{J}_z$, with eigenvalues $\hbar^2 J(J+1)$ and $\hbar M$, respectively, are obtained by applying the operator

$$\hat{P}^J_{MK} = \frac{2J+1}{16\pi^2} \int_0^{4\pi} d\alpha \int_0^{\pi} d\beta \, \sin(\beta) \int_0^{2\pi} d\gamma \, \mathcal{D}^{J*}_{MK} \hat{R}, \quad (4)$$

where $\hat{R} = e^{-i\alpha\hat{J}_z} e^{-i\beta\hat{J}_y} e^{-i\gamma\hat{J}_z}$ is the rotation operator and $\mathcal{D}^J_{MK}(\alpha, \beta, \gamma)$ is a Wigner function[1] [50]. $\hat{P}^J_{MK}$ picks the component with angular momentum projection K along the intrinsic z axis. The projected state is then obtained by summing over all K components of the mean-field state $|q\rangle$,

$$|JM\kappa q\rangle = \sum_{K=-J}^{+J} f^J_\kappa(K) \, \hat{P}^J_{MK} |q\rangle = \sum_{K=-J}^{+J} f^J_\kappa(K) \, |JMKq\rangle, \quad (5)$$

with weights $f^J_\kappa(K)$ determined by minimizing the energy [5,6] (see the following). The number of values that the index κ can take is restricted by the symmetries of the mean-field states [13] (signature with respect to x and time-reversal invariance) to $J+1$ for even J values and $J-1$ for odd J values.

Note that $\hat{P}^J_{KM}$ is not a projector in the strict mathematical sense, but it has the properties $\hat{P}^J_{KM}\hat{P}^{J'}_{M'K'} = \delta_{JJ'}\delta_{MM'}\hat{P}^J_{KK'}$ and $(\hat{P}^J_{KM})^\dagger = \hat{P}^J_{MK}$ [51].

---

[1]Alternatively, the integration intervals can be chosen as $\alpha \in [0, 2\pi]$, $\beta \in [0, \pi]$, and $\gamma \in [0, 4\pi]$. In any case, for systems with integer J values as discussed here, the integration over $[2\pi, 4\pi]$ of either α or γ gives just a factor of 2.

C. Mixing of states with different deformations

The fluctuations of the intrinsic deformation and the resulting spreading of the nuclear states in the β-γ plane can be described by a superposition of angular-momentum projected states by using the two intrinsic quadrupole degrees of freedom q as generator coordinates. Taking into account that one has also to mix all K values for each deformation, one obtains a resulting wave function given by

$$|JM\nu\rangle = \sum_q \sum_K F^J_\nu(K, q)|JMKq\rangle. \quad (6)$$

This corresponds to the discretized version of the GCM. $F^J_\nu(K, q)$ is a weight function of the K components of the angular-momentum projected states of intrinsic deformation q, determined from

$$\frac{\delta}{\delta F^{J*}_\nu(K, q)} \frac{\langle JM\nu|\hat{H}|JM\nu\rangle}{\langle JM\nu|JM\nu\rangle} = 0, \quad (7)$$

which leads to the Hill-Wheeler-Griffin (HWG) Eqs. [52,53]

$$\sum_{q'} \sum_{K'} \big[\mathcal{H}_J(K, q; K', q') \\ - E^J_\nu \mathcal{I}_J(K, q; K', q') \big] F^J_\nu(K', q') = 0, \quad (8)$$

with the energy and norm kernels

$$\mathcal{H}^J(K, q; K', q') = \langle JMKq|\hat{H}|JMK'q'\rangle, \quad (9)$$
$$\mathcal{I}^J(K, q; K', q') = \langle JMKq|JMK'q'\rangle. \quad (10)$$

For the sake of simple notation, we have introduced the method using a Hamilton operator $\hat{H}$. We shall comment on the procedure used to calculate the Hamiltonian kernels from an energy density functional and discuss some problems this may cause in Sec. II F.

The dimension of the variational space is considerably increased by introducing triaxial deformation. One cannot limit the angular momentum projection to $K = 0$, and several K components for each deformation have to be mixed. This has to be done with some care because of the high redundancy of the GCM bases, in the K space for a given deformation on the one hand and also for the whole set of deformations on the other hand. For an efficient elimination of redundant states we have chosen a four-step procedure. We start from a basis $|JMKq\rangle$. First, we restrict the subspace for each deformation q and angular momentum J by diagonalizing the norm kernel $\mathcal{I}^J(K, q; K', q)$, rewritten in its significant subspace [13], and neglecting eigenstates with negligible eigenvalues, typically smaller than 10^{-3}. Second, we solve the HWG equation in K space within this new basis. The solutions $|JM\kappa q\rangle$ are labeled by an index κ, Eq. (5). The number of values that κ can take for a given J depends on the deformation. It is just one for axial states and even J values and is usually larger for triaxial deformation. In a third step, we transform all matrix elements to the new basis $|JM\kappa q\rangle$ and diagonalize the norm matrix $\mathcal{I}^J(\kappa, q; \kappa', q')$ in the combined κ and q space. Once more, only significant eigenvectors of the norm matrix are retained. Finally, the Hamiltonian kernel is diagonalized in the basis of norm eigenstates to construct the weight functions $F^J_\nu(\kappa, q)$. The final eigenstates $|JM\nu\rangle$, Eq. (6), mix all K and q values.

They are then used to calculate all observables and transition moments.

Note that our method is not restricted to the choice of the triaxial quadrupole moment as a generator coordinate. This choice is suggested by the importance of quadrupole correlations in nuclei, but any other collective variable associated with an even multipole moment could be additionally considered, at the expense of having a larger mean-field basis. Including odd multipoles, in particular octupole deformations, would require a relatively simple generalization of the codes but cannot be considered at present. However, some modes not related to a shape degree of freedom, such as pairing vibrations, can be included without modification of the numerics, as done earlier without angular momentum projection in Refs. [28–30].

D. Electromagnetic matrix elements

Once the HWG equation is solved and the weight functions $F_\nu^J(\kappa, q)$ are known, the expectation values and transition moments of other observables $\hat{O}$ can be determined by starting from the kernels $\langle JMKq|\hat{O}|JMK'q'\rangle$ of the corresponding operators. Some of them provide a good test of the accuracy of symmetry restoration, which can be used to determine a sufficient number of points for projection. The matrix elements of the proton and neutron number operators, for example, are equal to the required values with an absolute deviation lower than 10^{-8}, and they have a dispersion lower than 10^{-8} when using a nine-point formula for the particle-number projection.

The symmetries of the unrotated time-reversal invariant HFB states (time reversal and triaxiality) permit the reduction of the integration intervals for Euler angles to $\alpha \in [0, \pi/2]$, $\beta \in [0, \pi/2]$, and $\gamma \in [0, \pi]$ (i.e., 1/16 of the full $8\pi^2$ integration volume for systems with integer spin). The integrals over α and γ are discretized with a trapezoidal rule, while for β we employ Gauss-Legendre quadrature. The number of points in these intervals used for the results reported in the following is 6 for α, 18 for β, and 12 for γ, which corresponds to 24, 36, and 24 points in the full $8\pi^2$ integration volume necessary for integer J values. With this discretization, the calculated expectation values of the angular momentum operators $\hat{J}^2$ and $\hat{J}_z$ are accurate with an error of the order 10^{-4} for the values of J discussed here.

Since the restoration of rotational symmetry provides wave functions in the laboratory frame of reference, one can compute directly the expectation values and transition matrix elements of electromagnetic operators. Besides mean-square radii and $E0$ transition moments, we calculate spectroscopic quadrupole moments and $B(E2)$ values as well as magnetic moments and $B(M1)$ values. By combining projection and variational GCM mixing of states with different mass quadrupole moments, the $B(E2)$ transition moments for in-band and out-of-band transitions take the form

$$B(E2; J'_{\nu'} \to J_\nu) = \frac{e^2}{2J'+1} \sum_{M=-J}^{+J} \sum_{M'=-J'}^{+J'} \times \sum_{\mu=-2}^{+2} |\langle JM\nu|\hat{Q}_{2\mu}|J'M'\nu'\rangle|^2 \quad (11)$$

and the spectroscopic quadrupole moments are given by

$$Q_s(J_\nu) = \sqrt{\frac{16\pi}{5}} \langle JM = J \nu|\hat{Q}_{20}|JM = J \nu\rangle. \quad (12)$$

The matrix elements of the electric quadrupole moment operator $Q_{2\mu} = e \sum_p r_p^2 Y_{2\mu}(\Omega_p)$ that enter the $B(E2)$ values and Q_s are calculated by using point protons with their bare electric charge e. This approach is justified by the following considerations. First, there is no empirical evidence that electric moments are significantly modified by the in-medium effects that are absorbed into the effective energy functional but ignored for all other observables. Second, we use the entire space of occupied single-particle states without assuming an inert core. Third, the projected GCM, as a "horizontal expansion" [54] of large-amplitude dynamics, can be formulated such that the calculation of matrix elements does not contain a sum over unoccupied states [20,22,55]. The absence of effective charges is an important feature of a method aiming at a universal description of nuclei. The (at least approximate) folding with the intrinsic charge distribution of protons and neutrons to construct a charge density is important for radii [1], but it plays no role for multipole moments when accepting the current precision of our approach.

Both the $B(E2)$ and Q_s values scale with mass and angular momentum. With triaxial shapes, however, one can no longer define a dimensionless intrinsic deformation β_2 that corresponds to a single Q_s or a single $B(E2)$ value, as can be done in the axial case [35], as one needs two independent observables (i.e., that are not within the same band) to determine the deformation β_2 and the angle γ [56].

Similarly, magnetic moments are given by

$$\mu(J_\nu) = \langle J, M = J, \nu|\hat{\mu}_{10}|J, M = J, \nu\rangle \quad (13)$$

and $B(M1)$ values are obtained as

$$B(M1; J'_{\nu'} \to J_\nu) = \frac{3}{4\pi} \frac{1}{2J'+1} \sum_{M=-J}^{+J} \sum_{M'=-J'}^{+J'} \times \sum_{\mu=-1}^{+1} |\langle JM\nu|\hat{\mu}_\mu|J'M'\nu'\rangle|^2. \quad (14)$$

The magnetic dipole operator $\hat{\boldsymbol{\mu}}$ entering both expressions is given by

$$\hat{\boldsymbol{\mu}} = g_{\ell,p}\hat{\mathbf{L}}_p + g_{s,p}\hat{\mathbf{S}}_p + g_{s,n}\hat{\mathbf{S}}_n, \quad (15)$$

where $\hat{\mathbf{L}}_t$ and $\hat{\mathbf{S}}_t$ are the total orbital and spin operators for protons and neutrons, $t = p, n$, and $g_{\ell,p} = 1 \mu_N$, $g_{s,p} = 5.585 \mu_N$, and $g_{s,n} = -3.826 \mu_N$ are the g factors of protons and neutrons in units of the nuclear magneton μ_N. Unlike the electric moments, the spin contribution to the magnetic moments is modified by the physics of short-range correlations, which is resummed into the energy functional but not explicitly considered in the wave functions. The spin g factors are often quenched by an empirical factor to mock up these effects. In the present paper, we start with time-reversal invariant mean-field states for which the spins of conjugated states exactly cancel each other. Although this is no longer the case after mixing such states, particularly when projecting

on angular momentum, the angular-momentum projected total spin $\langle JM = J\nu | \hat{S}_z | JM = J\nu \rangle$ remains a small correction of a few percent to the dominating collective contribution from orbital angular momentum when calculating the z component of total angular momentum in the laboratory frame, $\langle JM = J\nu | \hat{J}_z | JM = J\nu \rangle = \hbar J$. This has two consequences. First, we can ignore the subtlety of in-medium corrections to the spin g factors for the time being. However, when projecting and mixing cranked states at high spin or n-quasiparticle states that might have significant open spin, this point will deserve more attention. Second, the magnetic moments calculated for the projected and mixed states discussed in the present paper will be very close to the expectation value of the proton orbital angular momentum $\langle JM = J\nu | \hat{L}_{z,p} | JM = J\nu \rangle$ in nuclear magnetons.

E. Evaluation of kernels

The matrix elements that are needed to solve the HWG equation and to calculate the electromagnetic properties of the GCM eigenstates are matrix elements of tensor operators $\hat{T}_{\lambda\mu}$ of rank λ between particle-number and angular-momentum projected states $\langle q | \hat{P}^N \hat{P}^Z \hat{P}^J_{KM} \hat{T}_{\lambda\mu} \hat{P}^{J'}_{M'K'} \hat{P}^Z \hat{P}^N | q' \rangle$. As at present we consider only operators that commute with the particle-number operator; the particle-number projector for the left state can be commuted with $\hat{T}_{\lambda\mu}$ and one only has to project the right state on particle number. The angular-momentum projection operator, however, does not commute with tensor operators of rank different from zero. Still, the commutator can be evaluated by using angular-momentum algebra to obtain matrix elements with an angular-momentum projection operator acting on the left state only:

$$\langle q | \hat{P}^J_{KM} \hat{T}_{\lambda\mu} \hat{P}^{J'}_{M'K'} | q' \rangle$$
$$= \frac{2J'+1}{2J+1} (J'\lambda J | M'\mu M) \sum_{k=-J}^{+J} (J'\lambda J | K', K'-k, k)$$
$$\times \langle q | \hat{P}^J_{Kk} \hat{T}_{\lambda, K'-k} | q' \rangle. \qquad (16)$$

For a scalar operator $\hat{T}_{00}$, this simplifies to

$$\langle q | \hat{P}^J_{KM} \hat{T}_{00} \hat{P}^{J'}_{M'K'} | q' \rangle = \delta_{JJ'} \delta_{MM'} \langle q | \hat{P}^J_{KK'} \hat{T}_{00} | q' \rangle. \quad (17)$$

As a consequence, we have to evaluate matrix elements of the form

$$\langle q | \hat{R}^\dagger(\alpha, \beta, \gamma) \hat{T}_{\lambda\mu} e^{i\phi_n \hat{N}} e^{i\phi_z \hat{Z}} | q' \rangle = \langle L | \hat{T}_{\lambda\mu} | R \rangle, \qquad (18)$$

where $|q\rangle$ and $|q'\rangle$ are HFB states with possibly different intrinsic deformations, and $|L\rangle$ and $|R\rangle$ are the HFB states rotated in coordinate and gauge space, respectively. Key elements of the evaluation of these kernels are outlined in the Appendix.

F. Configuration mixing using energy functionals

For the sake of simplicity, we have outlined the projected GCM using a many-body Hamilton operator. In practice, however, an energy density functional is used in a form postulated by analogy with the Hamiltonian case [20,57].

In this procedure, the multi-reference (MR) energy density functional (EDF) is obtained by replacing the density matrices in the single-reference energy functional by the transition density matrices as they appear when transition matrix elements of a Hamilton operator are evaluated with the generalized Wick theorem [5,20,58]. The terms in the Skyrme EDF that contain time-odd densities are treated as described in Appendix C of Ref. [20] and give a small contribution to the nondiagonal kernels. The density-dependent terms are generalized by using the standard prescription that the density is replaced by the transition density in the density-dependent terms. This is the only prescription that guarantees various consistency requirements of the energy functional [38,59]. However, this procedure may lead in some cases to problems that have become evident recently [60,61]. Discontinuities or even divergences of the energy kernel may indeed appear as a function of deformation. A regularization scheme has been proposed [62] and applied to a simple case of MR-EDF calculations [63]. However, it cannot be applied to the standard form of the Skyrme and Gogny interactions [64]. We leave this problem to be addressed in the future and stick to a standard Skyrme energy functional, as done in our earlier studies.

III. ^{24}MG AS AN ILLUSTRATION

The main features of our method are exemplified by a calculation for ^{24}Mg. We use the parametrization SLy4 [65] of the Skyrme + Coulomb energy density functional for the particle-hole channel of the effective interaction, supplemented by a zero-range density-dependent pairing energy functional [66]. A soft cutoff around the Fermi energy is used when solving the HFB equations as introduced in Ref. [67].

Figure 1 provides as a reference some key results from an *axial* calculation as a function of the dimensionless mass quadrupole deformation given through Eq. (3). In this figure, oblate shapes are labeled by negative values of β_2. On the top part we compare the variation of the energy with deformation obtained by projecting on particle numbers N and Z only (solid line) and by projecting on particle number and on $J = 0$ (dotted line). In the bottom part, the Nilsson diagram of eigenvalues of the proton single-particle Hamiltonian is shown. The Nilsson diagram for neutrons is nearly identical to the one for protons, except for a global shift owing to the absence of the Coulomb potential. The projection on $J = 0$ significantly increases the energy gain from deformation. The mean-field configuration corresponding to the minimum also has a significantly larger prolate deformation after projection than before. After projection, the axial minimum corresponds to the intrinsic deformation where the $Z = N = 12$ gap in the Nilsson diagram is largest. The Nilsson diagram indicates also that there are only very few level crossings in the interesting region of deformations.

A. Triaxial energy maps

Three (β, γ) deformation energy surfaces for ^{24}Mg are displayed in Fig. 2. All energies are normalized to the energy of the spherical configuration. A projection on particle numbers
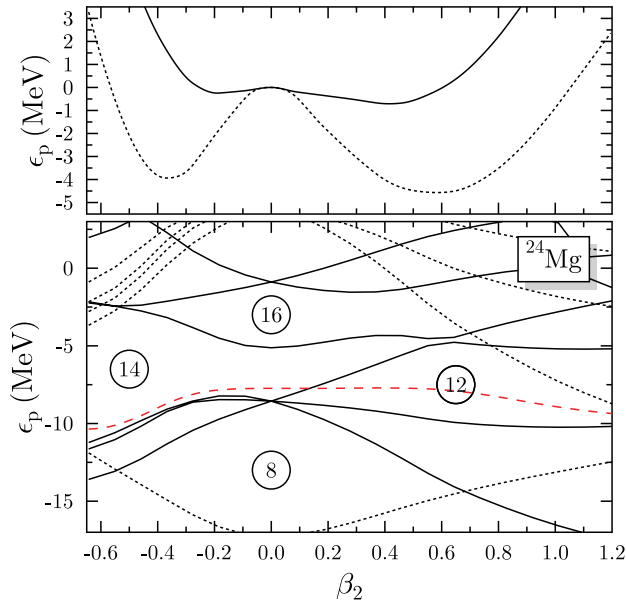
FIG. 1. (Color online) Lower panel: Nilsson diagram of the eigenvalues of the proton single-particle Hamiltonian for axial shapes. Solid lines denote levels with positive parity, dotted lines levels with negative parity, and the red dashed line the Fermi energy. Upper panel: Particle-number projected (solid line) and particle-number and angular-momentum $J = 0$ projected (dotted line) axial deformation energy curves.
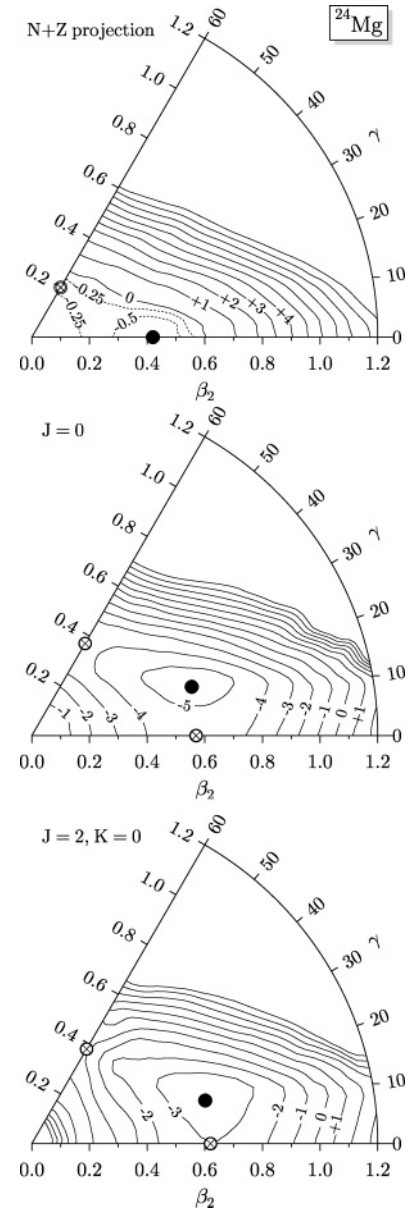

FIG. 2. Triaxial quadrupole energy maps obtained by projecting mean-field configurations on N and Z only (top) and also either on $J = 0$ (middle) or on $J = 2$ and $K = 0$. In the latter case, the z axis is chosen as the symmetry axis. Filled circles denote minima; the $\otimes$ symbols denote saddle points. All energies are normalized with respect to the energy of the particle-number projected spherical state.

N and Z is performed for all three panels; it is combined with a projection on the angular momentum $J = 0$ in the middle panel and on $J = 2$ and $K = 0$ on the lower one. Several comments on the interpretation of the deformation energy surfaces are in order. First, the coordinates β_2 and γ are not related to any matrix element in the angular-momentum projected energy surfaces but merely provide a label for the intrinsic state from which the projected energy is obtained. All states projected on $J = 0$ are spherical in the laboratory frame. Second, neither the mean-field nor the projected states are orthogonal, such that the energy maps do not and cannot represent the actual metric, which is related to the inverse of the respective overlap matrix. Finally, the $J = 2$, $K = 0$ surface depends on the orientation chosen for the principal axes of the nucleus. The quadrupole moment along the z axis is the largest one in Fig. 2. We shall show later that the $K = 0$ results have no obvious interpretation for other choices.

Starting with the energy surface without angular-momentum projection, one sees that the mean-field ground state corresponds to an axial prolate deformation, more bound than the spherical configuration by about 700 keV. Comparing with the axial energy curve given as a solid line in the upper panel of Fig. 1, one notices that the prolate minimum is indeed a true one but that the oblate extremum seen in Fig. 1 is a saddle point in the γ direction. A qualitatively similar deformation energy surface was found in HF + BCS calculations with the Skyrme interaction SIII in Ref. [68] and in HFB calculations with the Gogny force D1 in Ref. [69].

The projection on $J = 0$ favors triaxial configurations: The lowest energy is obtained for a triaxial mean-field

configuration with $\gamma \approx 16°$ and a value for β_2 around 0.6, similar to that of the axial mean-field state giving the lowest $J = 0$ projected energy. Before projection, these two states were separated by 2.2 MeV. The energy gain for the triaxial point is 3.1 MeV larger than that of the axial point. This difference is thus large enough to compensate for the difference in energy between the mean-field configurations. However, this result has to be taken *cum grano salis* as the deformation has a limited meaning after projection. In particular, the states resulting from the projection on the same J value of mean-field configurations corresponding to different quadrupole moments may have a large overlap. The states with the lowest energy

obtained after projection of axial and triaxial configurations have an overlap close to 0.9. ^{24}Mg is one of the few light nuclei with a deformed mean-field ground state when pairing correlations are taken into account. In this small system, however, the static quadrupole correlation energy (i.e., the deformation energy of the mean-field ground state) is much smaller than the dynamical quadrupole correlation energy obtained from projection and mixing of states with different intrinsic shapes; this is a general feature of light nuclei with $A < 100$ [70].

The projection on $J = 2$, $K = 0$ leads to an energy map whose interpretation is more difficult than that for $J = 0$. The orientation of the nucleus that is chosen gives this energy map some meaning in the interpretation of the first 2^+ level, whereas the second 2^+ state belongs mainly to the map corresponding to $K = 2$. The topography of the $J = 2$, $K = 0$ map is quite similar to, but slightly flatter than, that of the $J = 0$ energy map.

We will not show here the deformation energy surfaces for higher J and K values. When starting with time-reversal invariant mean-field states, the angular-momentum projected energy surfaces for all even values of J and $K \neq 0$ are infinite at $\gamma = 0°$ and degenerate with the $K = 0$ surface of the same J for $\gamma = 60°$, which we will exemplify for one oblate configuration in the next section. As a consequence, K mixing becomes usually much stronger when going from prolate to oblate shapes with increasing γ. For odd values of J, there is no $K = 0$ component, and the energy surfaces for finite K are infinite at both $\gamma = 0°$ and $\gamma = 60°$.

These findings are consistent with what has been seen before. Many even-even nuclei have a quadrupole-deformed mean-field ground state with a substantial energy gain that might be as large as 25 MeV in very heavy nuclei [70]. The corresponding shape in the intrinsic frame, however, remains axial in most cases. Triaxial ground-state deformation is rare at the mean-field level, and the additional energy gain from nonaxial deformation is usually quite small compared to the deformation energy of the axial minimum or saddle in the same nucleus [69,71–74]. Triaxiality, however, plays an important role for high-spin states when described in mean-field approaches [75,76]. The situation changes when going beyond the mean field. It is well known that projection on good quantum numbers favors the breaking of the corresponding symmetries in the underlying mean-field states: For a nucleus with a spherical minimum in the mean-field deformation energy surface, angular-momentum projection on $J = 0$ results in a deeper minimum at slightly deformed shapes [70], as first noticed by Dalafi [77]; for a nucleus with an axial minimum of the mean-field energy surface, the minimum of the $J = 0$ angular-momentum projected energy surface is slightly shifted into the triaxial plane, as has been demonstrated by Hayashi *et al.* [11].

B. Angular-momentum projection of a single triaxial HFB state

1. The role of the orientation in the intrinsic frame

Scalar quantities such as the overlap and the energy kernels of the GCM do not depend on the orientation of the projected state in the laboratory frame (i.e., on its angular momentum

projection M). Moreover, final results do not depend on the orientation of the mean-field state in its intrinsic frame when time-reversal invariance is preserved. This equivalence, however, is only obtained after K mixing. This provides the opportunity to analyze the role of K mixing for the projection of states with the same intrinsic deformation but a different orientation of their principal axes. It also constitutes an excellent test of the numerical accuracy of the projection scheme that we have developed.

There are six possible ways to orient a triaxial nucleus in its intrinsic frame in such a way that the major axes of the intrinsic quadrupole moment coincide with the axes of the intrinsic coordinate system. These six possibilities correspond to the six sextants of the β-γ plane. Owing to the particular role played by the intrinsic z axis in the angular-momentum projector [Eq. (4)], results are invariant under exchange of the x and y axes such that they give pairwise the same decomposition $|JMKq\rangle$. It is, therefore, sufficient to consider the intrinsic z axis coinciding with the longest, intermediate, or shortest axis of the triaxial state, without specifying the orientation of the other two axes. The results for excitation energies and $B(E2)$ values obtained for the three possible orientations of the nucleus are presented in Fig. 3; key numbers for excitation energies are repeated in Table I. When the intrinsic long axis is chosen along the z axis (left panel), K mixing has a small effect and a clear connection can be made between the $K = 0$ and the $K = 2$ bands and the ground-state and γ bands after mixing. The differences between the results before and after K mixing are due to the nonorthogonality of the states $|JMKq\rangle$ with the same J and M values but different K, which is removed in the orthogonal basis $|JM\kappa q\rangle$. This orthogonalization pushes up the second 4^+ state by 1 MeV. The dominating in-band $B(E2)$ values are similar before and after K mixing, whereas the much smaller out-of-band $B(E2)$ values change substantially.

TABLE I. Excitation energies after decomposition of the mean-field state that gives the minimum of the $J = 0$ projected energy surface into angular-momentum projected components $|JMKq\rangle$ and after K mixing into $|JM\kappa q\rangle$ for three different orientations of the same triaxial state in the intrinsic frame, corresponding to Fig. 3.

J	K	\multicolumn{3}{c}{Decomposition}	κ	\multicolumn{3}{c}{K mixing}
		104°	136°	16°		104°	136°	16°
0	0	0.00	0.00	0.00	1	0.00	0.00	0.00
2	0	4.86	3.86	1.83	1	1.84	1.83	1.83
	2	2.21	2.40	7.07	2	7.24	7.25	7.24
3	2	9.63	9.62	9.61	1	9.63	9.62	9.61
4	0	9.85	7.68	5.45	1	5.47	5.44	5.44
	2	7.89	6.66	10.29	2	11.39	11.35	11.34
	4	6.31	6.63	16.56	3	–	–	–
5	2	18.34	16.14	14.52	1	14.47	14.42	14.42
	4	14.85	14.82	20.53	2	–	–	–
6	0	15.59	14.82	11.09	1	11.11	11.08	11.06
	2	14.14	12.84	14.27	2	17.25	17.38	17.18
	4	13.75	11.94	20.58	3	–	–	–
	6	11.95	12.94	29.26	4	–	–	–

FIG. 3. Excitation spectra and selected $B(E2)$ values after decomposition of the mean-field state that gives the minimum of the $J=0$ projected energy surface into angular-momentum projected components $|JMKq\rangle$ (left) and after K mixing into $|JM\kappa q\rangle$ (right) for three different orientations of the same triaxial state in the intrinsic frame.

The situation is quite different when the triaxial mean-field state is orientated in such a way that the z axis is not the longest one. The energies and transition probabilities obtained before K mixing have no obvious correspondence with the K-mixed results. In particular, the $B(E2)$ values without K mixing are of similar size for in-band and out-of-band transitions. However, both Fig. 3 and Table I clearly indicate the independence of the results from the orientation of the mean-field state after K mixing. Note that the 3^+ level is not affected by K mixing; as with good time-reversal invariance, there is only one independent nonzero K component with $K=2$.

Figure 4 presents the decomposition of the norm of the same states as in Fig. 3 in components with different total angular momenta J,

$$c_J^2 = \sum_{K=-J}^{+J} \langle q|\hat{P}_{KK}^J|q\rangle, \qquad (19)$$

summed over all possible values of K; Fig. 5 shows the decomposition into components with different intrinsic angular

momentum projection K,

$$c_K^2 = \sum_{J \geqslant |K|} \langle q|\hat{P}_{KK}^J|q\rangle, \qquad (20)$$

summed over all possible values of J for a given value of K. The underlying state $|q\rangle$ is assumed to be particle-number projected and normalized. As we always choose an orientation of the triaxial state $|q\rangle$ where the intrinsic z axis coincides with one of the principal axes, the components of opposite K have the same weight $c_{+K}^2 = c_{-K}^2$. Furthermore, all components with an odd value of K are zero for all values of J.

The decomposition of a triaxial mean-field state into components with different J values in the laboratory frame should be independent of its orientation in the intrinsic frame, which is indeed the case within the resolution of Fig. 4. The plot suggests a separation of the coefficient c_J^2 into two distinct curves: one for even values of J, which dominates the decomposition and peaks for $J=2$, and a second much weaker one for odd values of J, which peaks at $J=3$. (When decomposing a time-reversal invariant state, there is no component with $J=1$ for symmetry reasons.) Increasing the deformation of the intrinsic state modifies the c_J^2 distribution

FIG. 4. Decomposition of the mean-field state that gives the minimum of the $J=0$ projected energy surface into components of same angular momentum J, Eq. (19). The results obtained from the different possible orientations in the intrinsic frame are undistinguishable.

FIG. 5. Decomposition of the mean-field state that gives the minimum of the $J=0$ projected energy surface into components of same K, Eq. (20), for three different orientations of the state in the intrinsic frame.

such that the peaks of the distributions for even and odd J are shifted toward larger values of J.

By contrast, the decomposition of the same triaxial intrinsic state into its K components depends strongly on its orientation, which underlines that K is not an observable quantity. The distribution of K components is quite narrow when the long axis of the intrinsic state coincides with the z axis, and it becomes broader when the intermediate or even short axis is chosen instead. The different distributions in K space indicate that the numerical convergence of angular-momentum projection is not the same for all possible orientations of the mean-field state. The accurate determination of components with large K values requires many integration points for the Euler angles α and γ; hence, it is more favorable to orient the mean-field wave function with its z axis along the long axis. The sum over all c_J^2 coefficients should be equal to the sum over all the c_K^2 ones and equal to 1. There is, in practice, a slight numerical deviation of the order of 10^{-5}, which can be attributed to high-J and high-K components requiring a higher number of integration points than have been used here.

2. Decomposition of an oblate HFB state

A further test of our method is given by the projection of an oblate mean-field configuration, for which the symmetries of our codes allow two distinct orientations in its intrinsic frame: The z axis can be either the symmetry axis or perpendicular to it. Using the properties of the transformation of the operator $\hat{P}_{MK}^J$ under rotation, one can show that a pure $K = 0$ state is transformed into a multiplet of states with K between 0 and J. However, the transformed wave functions differ only by an unobservable phase and are degenerate. An example is given in Fig. 6 for the mean-field state with mass quadrupole moment $Q_0 = 80$ fm^2, which gives the axial oblate saddle point of the $J = 0$ projected energy surface. When using the z axis
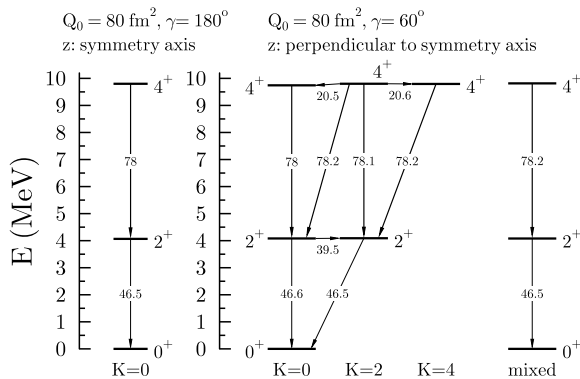

FIG. 6. Excitation spectra and selected $B(E2)$ values after decomposition of the mean-field state that gives the axial oblate saddle of the $J = 0$ projected energy surface into angular-momentum projected components $|JMKq\rangle$. The left panel provides the decomposition when choosing the z axis as the symmetry axis, $\gamma = 180°$. The middle panel gives the decomposition into K components when the symmetry axis is chosen perpendicular to the z axis. The right panel shows the unique band resulting from K mixing (see text).

TABLE II. Spectroscopic quadrupole moments obtained from projection without and with K mixing compared with values obtained from the asymmetric rotor model. In this latter case, the intrinsic charge quadrupole moment $Q_{0,p} = 63.45$ e fm^2 ($\beta_p = 0.583$) and $\gamma = 16.1°$ value of the triaxial HFB state are used as input.

Quantity	No mixing	K mixing	Rotor
$Q_s(2_1^+)(e$ fm$^2)$	−19.1	−18.7	−17.0
$Q_s(2_2^+)(e$ fm$^2)$	20.0	18.1	17.0
$B(E2, 2_1^+ \rightarrow 0_1^+)(e^2$ fm$^4)$	94.9	95.7	75.5
$B(E2, 2_2^+ \rightarrow 0_1^+)(e^2$ fm$^4)$	15.9	5.2	4.6
$B(E2, 2_2^+ \rightarrow 2_1^+)(e^2$ fm$^4)$	8.4	26.4	14.3
$B(E2, 3_1^+ \rightarrow 2_1^+)(e^2$ fm$^4)$	11.6	10.0	8.3
$B(E2, 3_1^+ \rightarrow 2_2^+)(e^2$ fm$^4)$	146.4	165.4	134.7

as symmetry axis, as was done in axial calculations [34–41], the projection decomposes the mean-field state into a single rotational band of $K = 0$ states; all other K components have zero norm. When orienting the intrinsic state such that the z axis is perpendicular to the symmetry axis, as done at $\gamma = 60°$ in the β-γ plane, all even K components $|JMKq\rangle$ up to $K = J$ are nonzero for each J. When constructing the $|JM\kappa q\rangle$ states, however, the diagonalization of the norm matrix gives only one nonzero eigenvalue per even J, and one ends up with the same rotational band as obtained by exploiting the symmetry of the intrinsic state.

3. Comparison with the asymmetric rotor model

The spectroscopic quadrupole moments and $B(E2)$ values obtained by the projection of a triaxial mean-field state are mainly determined by its geometry. This property is illustrated in Table II where we compare the values obtained by projecting the same triaxial mean-field state as in Fig. 3 to those calculated with the asymmetric rotor model introduced by Davydov and co-workers [78,79], using the intrinsic proton quadrupole moment $Q_{0,p} = 63.45$ e fm^2 ($\beta_p = 0.583$) and $\gamma = 16.1°$ as input. The agreement is excellent and, in practice, improves with deformation.

C. Configuration-mixing calculations

1. Selection of the mean-field basis

As a last step, we perform a mixing of states obtained by projecting on particle-number and angular-momentum mean-field wave functions covering the full β-γ plane. Specifically, the results will be analyzed by comparing the spectra and transition probabilities obtained in calculations using four different subspaces of states:

(i) a basis of "prolate" axial states, comprising the four deformations $(q_1, q_2) = (80, 0)$, $(120, 0)$, $(160, 0)$, and $(200, 0)$ fm^2;

(ii) a basis of "axial" states, where two oblate deformations $(q_1, q_2) = (0, 80)$ and $(0, 120)$ fm^2 are added to the prolate basis;

(iii) a basis of six "triaxial" mean-field configurations $(80, 40)$, $(120, 40)$, $(160, 40)$, $(200, 40)$, $(80, 80)$, and $(120, 80)$ fm^2;

(iv) a basis labeled "full" where, depending on J, two to four states of the prolate basis are added to the triaxial basis.

For the full basis, we have added for each J value the largest possible number of axial points to the triaxial basis. We have excluded from the GCM calculations those deformed states that are situated in a region affected by the difficulties mentioned in Sec. II F. This region spreads from small deformations around the spherical point to a region with larger deformations between the oblate axis and $\gamma \approx 50°$. This restriction does not permit the mixing of triaxial and oblate axial states.

For ^{24}Mg, the number of axial states that can be added to the set of triaxial states is not large, just two to four, depending on the value for J. Redundancies appear very quickly in the norm kernel when more states are added to the nonorthogonal basis. This very small number of nonredundant states is a direct consequence of the very few level crossings visible in Fig. 1; even states with quite different intrinsic deformation might have a very similar single-particle spectrum. This feature is illustrated in Fig. 7, where the eigenvalues of the $J = 0$ norm kernel are plotted as a function of the number of states included in the configuration-mixing calculation. We start on the left of the figure with the eigenvalues of calculations performed in the prolate and axial bases. The addition of oblate configurations to the prolate set brings one large eigenvalue, close to 1, and another one around 10^{-2}. The range of values obtained for a purely triaxial set is very similar to the axial set, although both bases have no vectors in common. Starting from the initial set of triaxial points, prolate points are added one after the other. There is, thus, one more eigenvalue after each addition and the trace of the norm, which is equal to the number of discretization points, is increased by 1. One can see that this increase of the trace is mainly distributed among the largest eigenvalues, which increase slightly. Each time, a new eigenvalue around
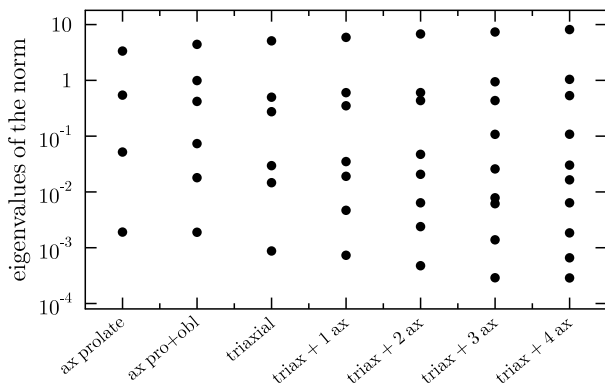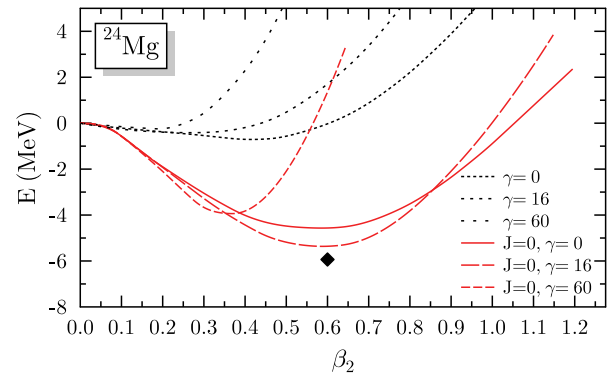

FIG. 8. (Color online) Deformation energy curve projected on N and Z (black) only and projected also on $J = 0$ (red) for three different values of γ, as indicated. The energies of the $J = 0$ GCM ground state obtained from the axial, triaxial, and full bases as described in the text cannot be distinguished within the resolution of the plot and are represented by the same filled diamond plotted at arbitrary deformation. All energies are normalized to that of the spherical particle-number projected state.

5×10^{-3} also appears, or an even smaller one when the fourth axial point is added. Although these changes are very small, the effect of the coupling between axial and triaxial states on all observables is not completely negligible.

2. Ground-state correlation energy

We have shown in Fig. 2 that the angular-momentum projection changes the topography of the $J = 0$ deformation energy surface and generates a minimum for the projection of a triaxial configuration. This result is illustrated further in Figure 8 where the variation of the energy along three cuts in the β-γ plane is plotted. The first curve corresponds to prolate deformations, $\gamma = 0°$, the second to oblate ones, $\gamma = 60°$, and the third to a cut along $\gamma = 16°$. Results obtained with and without projection on $J = 0$ are given. The big diamond covers the range of the GCM energies obtained by using the axial, triaxial, and full bases. The lowest energy corresponds to a prolate configuration in the nonprojected calculation, with triaxial energies always much larger than the prolate and oblate ones. After projection on $J = 0$, the triaxial curve is below the prolate one for a large range of deformations and the absolute minimum corresponds to a triaxial configuration about 800 keV more bound than the axial saddle point. However, the total energy gain obtained by mixing axial configurations is larger than that from the projection of a single triaxial configuration. Moreover, there is only a 35 keV difference between the energies obtained by the mixing of triaxial configurations and a further gain of 160 keV in the largest possible set of axial and triaxial configurations.

This result puts a limit on the meaning of "rotational" and "vibrational" energies in the ground state: What appears to be "vibrational" energy in a projected axial quadrupole GCM is transformed into "rotational" energy in a projected GCM including triaxial states. At the same time, this result is rather encouraging as it brings the hope that the ground-state correlation energies are rapidly saturating when more than

FIG. 7. Variation of the eigenvalues of the $J = 0$ norm kernel among different bases.

TABLE III. Comparison between the theoretical excitation energies in MeV and spectroscopic quadrupole moments in units of e fm^2 and the experimental values taken from Ref. [81].

Level	E_{ex}				Q_s			
	Axial	Triaxial	Full	Expt.	Axial	Triaxial	Full	Expt.
2_1^+	2.24	1.87	1.97	1.37	−17.1	−19.6	−19.4	−16.6(6)
4_1^+	5.88	5.44	5.57	4.12	−25.1	−26.1	−26.0	
2_2^+	7.69	6.88	6.99	4.24	9.9	17.1	16.6	
3_1^+	–	9.59	9.74	5.24	–	−0.1	−0.1	
4_2^+	13.29	11.12	11.28	6.01	9.0	−7.3	−7.4	
0_2^+	7.53	8.79	7.520	6.42	0.0	0.0	0.0	0.0

the restoration of symmetries on the axial mode is included. Hagino *et al.* [80] arrived at a similar conclusion while studying the ground-state correlation energy in an exactly solvable model that simulates collective quadrupole motion. Of course, systematic realistic calculations, in particular for heavier nuclei, are needed before a general rule can be established.

3. Excitation spectrum

The excitation spectra obtained in three different GCM bases are given in Fig. 9 and Table III. Table III also lists results for spectroscopic quadrupole moments, and the $B(E2)$ values for the most important transitions are given in Fig. 9. Experimental data are taken from Ref. [81] in both cases, and $5.940 \times 10^{-2} A^{4/3}$ e fm^4 = 4.11 e fm^4 is used for the $E2$ Weisskopf unit.

The spacing of levels, the relative strength of $B(E2)$ values, and the K content of the collective wave functions suggest a separation of the low-lying spectrum into three bands: the $\Delta J = 2$ ground-state band dominated by $K = 0$ components, a $\Delta J = 1$ γ band dominated by $K = 2$ components, and a third band that is again dominated by $K = 0$ components.

As already mentioned, the GCM ground-state energy is quite close in the purely axial and purely triaxial calculations, but it is 160 keV lower in the full calculation that combines triaxial and axial states. All excited levels, except the 0_2^+ one, are lower in the triaxial basis than in the axial one. Adding prolate axial states to the triaxial basis mainly lowers the energy of all 0^+ levels, pushing up levels with other values of J. The spectroscopic quadrupole moments Q_s and $B(E2)$ values, however, are not significantly affected.

The most significant difference between the axial and triaxial calculations concerns the first excited band, which is clearly a γ band in the triaxial basis. Odd-J levels are of course absent from the first excited band in the axial basis but some of the features of a γ band are already hinted in this band dominated by oblate configurations. In particular, the $B(E2)$ value for the transition from the 4_2^+ to the 2_2^+ level is very close to that of the triaxial calculation. This identification of the projection of an oblate state to a γ band was already suggested in Sec. III B2. However, K mixing does not bring any gain in energy in the projection of an oblate state since the relative weights of the K components are fixed by symmetry relations, whereas they are free to vary in the projection of triaxial states. The gain in energy brought by the inclusion of
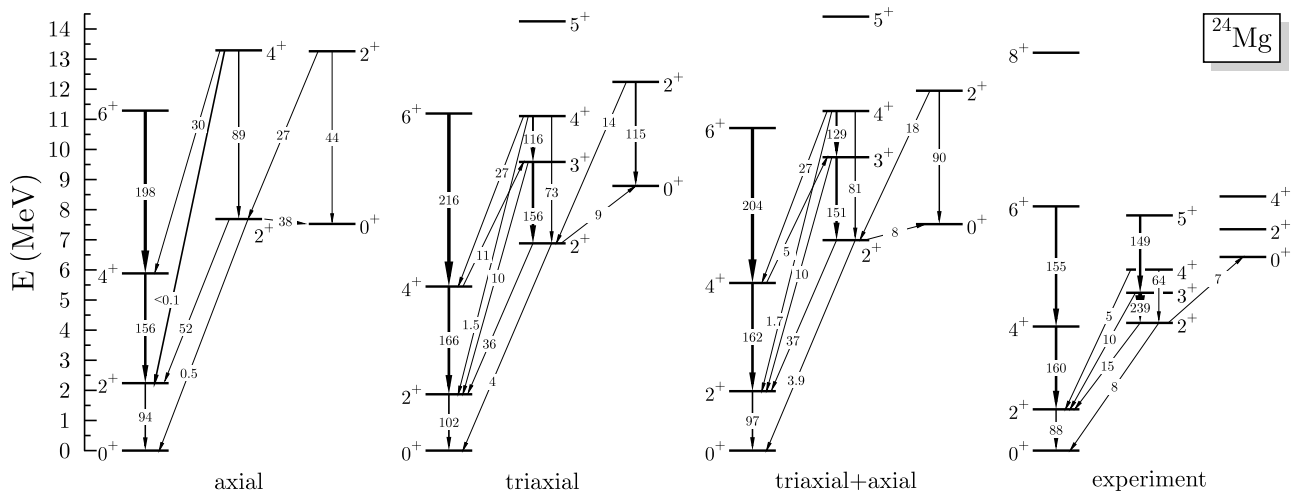

FIG. 9. Excitation spectra and $B(E2)$ values in e^2 fm^4 obtained in three of the bases defined in the text compared to the available experimental data. In the four cases, the spectrum is subdivided into a ground-state band, a γ band, and additional low-lying states that do not necessarily form a band.

TABLE IV. Overlaps between the GCM wave functions obtained in calculations using different sets of mean-field states. The two results marked by asterisks indicate that the number given represents the overlap between the second prolate and the third triaxial or full 2^+ excited states.

	Triaxial		Full	
	Prolate	Axial	Prolate	Axial
$J = 0$	0.97	0.99	0.97	0.99
	0.89	0.94	0.96	0.97
	0.16	0.93	–	0.96
$J = 2$	0.97	0.98	0.97	0.98
	0.21	0.86	0.23	0.88
	0.88*	0.82	0.88*	0.81

triaxial configurations is evident when looking at the energies and the spectroscopic quadrupole moment (Table III), which change drastically when going from the axial to the triaxial calculation.

The inclusion of triaxial deformations has also a strong effect on the energies of the levels in the second band. The excitation energy of the 2_2^+ level is lowered by nearly 1 MeV, and that of the excitation energy of the 4_2^+ level even more. Altogether, the inclusion of triaxial mean-field states brings the right tendency to make the spectrum more compact and brings it closer to the experimental data. It remains to verify whether the use of time-reversal invariance breaking HFB states will add the extra gain of energy required to bring the states with J different from 0 closer to the experimental levels. In particular, the odd-J states in the γ band still have excitation energies that are much too high.

To analyze further the equivalence of and differences between the bases that we have used, the component of the triaxial and full bases that are included in the prolate and axial bases are given in Table IV. These overlaps, $\langle J M \nu | J M \mu \rangle$, can be easily calculated by using the $F_\nu^J(\kappa, q)$ and the norm kernels $\mathcal{I}(\kappa, q; \kappa', q')$. A bit surprisingly, the differences between the collective ground-state wave functions obtained within the axial and full bases are very small, the overlap with the prolate basis being slightly lower but still quite high. The second 0^+ state is not as well described by the prolate basis and the third one state is missing in this basis. Note that the difference between the axial and full ground-state wave functions is still larger than the energy differences between these states (0.16 MeV out of a total energy of around 200 MeV).

The first 2^+ state has the same structure in all bases. In contrast, the second 2^+ state of the axial and full bases is not described by the prolate basis. Although the overlap between the 2_2^+ states in the axial and full bases is close to 0.9, the excitation energy is lowered by 800 keV when triaxial configurations are included. This confirms our previous interpretation that the mixing of prolate and oblate axial states can, to some extent, simulate states with $K \neq 0$, but not fully.

In the $N = Z$ nucleus ^{24}Mg, all calculated magnetic moments are just a few percent larger than $ZJ/(N + Z) = J/2$ in nuclear magnetons. This is a consequence of (a) the time-reversal symmetry that we impose on the underlying HFB

TABLE V. Comparison between theoretical and experimental $B(M1)$ values in units of μ_N^2. Data are taken from Ref. [81].

Transition	$B(M1)$			
	Axial	Triaxial	Full	Expt.
$2_2^+ \rightarrow 2_1^+$	4×10^{-6}	3×10^{-6}	3×10^{-6}	$1.6 \times 10^{-5}(14)$
$3_1^+ \rightarrow 2_1^+$	–	2×10^{-7}	1×10^{-7}	$3.8 \times 10^{-5}(20)$
$3_1^+ \rightarrow 2_2^+$	–	4×10^{-5}	4×10^{-5}	$6.2 \times 10^{-4}(30)$

states as explained in Sec. II D and of (b) the fact that protons and neutrons have nearly the same contribution to the angular momentum in this $N = Z$ nucleus. The calculated magnetic moments agree well with the available experimental ones [81] for the 2_1^+, 4_1^+, 2_2^+, and 4_2^+ states within the experimental error bars.

The calculated and experimental $B(M1)$ values are compared in Table V. Data are taken from Ref. [81] where $1.790 \, \mu_N^2$ is used for the $M1$ Weisskopf unit. The values that we obtain are about one order of magnitude too small, which clearly indicates that the projected currents and spin densities are underestimated. Starting from time-reversal breaking mean-field states instead of time-reversal invariant ones as done here can be expected to increase the $B(M1)$ values.

IV. SUMMARY AND OUTLOOK

A generalization of a method that enables the mixing of projected mean-field states that was previously limited to axial configurations has been set up to allow for a description of the full five-dimension quadrupole dynamics. Compared to a GCM calculation limited to projected axial quadrupole deformed states, the present method allows for a spreading of the collective states into the β-γ plane. In the case of ^{24}Mg, we have shown how the spectroscopic properties of the low-lying states are affected. One can summarize our main results as follows:

(i) When looking at the projection of a single configuration, the energy obtained for the ground state is significantly lowered when allowing for triaxial quadrupole deformation.

(ii) If one considers at the same time the correlation energy from symmetry restorations and configuration mixing, the total energy difference between the ground state obtained within an axial and a triaxial mean-field basis is quite small. This indicates that the nondiagonal matrix elements between prolate and oblate axially deformed mean-field states bring a large fraction of the correlation energy that is obtained by the projection of triaxial configurations between them. This puts a limit on the meaning of rotational and vibrational energies, as what appears to be "vibrational" energy in the projected quadrupole GCM of axial states is transformed into "rotational" energy in a projected GCM including triaxial

states. Of course, this result will have to be confirmed by studies in other nuclei.

(iii) This finding is also supported by the analysis of the spectrum of eigenvalues of the norm matrix, where adding triaxial states does not introduce states with large eigenvalues to the space of 0^+ states.

(iv) For higher J values, the situation is more complex. However, including triaxial deformations lowers the excitation energies and brings the spectrum closer to experiment.

On the basis of this analysis, one can draw some conclusions about the effect of triaxial deformations:

(i) Their effect on masses seems marginal and it is reassuring in some way: If one can confirm that triaxial deformations increase binding energies by only around 100 to 200 keV, it would be justified to avoid the complexities from their introduction in systematic mass calculations.

(ii) The gain of energy on excited states partly cures a problem common to all projected GCM calculations based exclusively on axial mean-field states. However, further improvements are still necessary, including the breaking of time-reversal invariance and the consideration of the projection of cranking states optimized for each angular momentum. The breaking of axiality is a necessary first step before the breaking of time-reversal invariance and we hope to validate the extension of our method in this case in the near future.

(iii) The power of our method will be more apparent when breaking of time-reversal invariance is included. Although some new states can already be described at the present level of development (e.g., odd-J members of $K \neq 0$ bands), it will be possible to describe quasiparticle excitations and in particular nuclei with an odd number of neutrons or protons.

(iv) Our method also provides an ideal tool to benchmark simpler models. To give only one example, the metric of the β-γ plane is generated directly in our method by the overlaps between mean-field wave functions of different shapes. Although it is not trivial to derive this metric in a multidimensional problem, as was done in Ref [20] for the one-dimensional case, it would be very instructive to compare a metric derived from a purely microscopic approach to the metrics that are usually based on semiclassical approximations.

There are no basic reasons that prevent the application of the method presented here to heavy nuclei, although this would be too time consuming with our current numerical implementation. Further developments are required to improve the efficiency of the numerical algorithms. In particular, the choice of discretization points used to evaluate the integrals over the Euler angles needs to be optimized and the codes have to be parallelized, which could be done in a very efficient way. Work in that direction is underway.

Another development that will have to be completed in the near future is the implementation of the regularization scheme proposed in Ref. [62] to remove the pathologies

brought by the use of the generalized Wick theorem when evaluating the energy kernels starting from an energy density functional. However, the conceptual and technical difficulties encountered in the present generalization of the projected GCM justify the continuation of the present developments in parallel. Considerable work at the level of the computational algorithm still remains to be performed to have a method applicable to heavy nuclei.

APPENDIX: COMMENTS ON THE NUMERICAL EVALUATION OF THE KERNELS

A. Self-consistent mean-field calculations

The mean-field states are generated with a simplified version of the cranked HFB code whose evolution is documented in Refs. [48,66,68]. We have imposed time-reversal invariance of the HFB vacua such that the single-particle wave functions are pairwise connected by time reversal. The single-particle wave functions are represented as complex spinors discretized on a three-dimensional Cartesian Lagrange mesh in coordinate space. In addition to time reversal, two further symmetries of the D_{2h}^{TD} symmetry group [82,83] are imposed on the single-particle basis, namely that they are eigenstates of the parity $\hat{P}$ and z signature $\hat{R}_z$. Their relative phases are fixed by choosing a basis where the eigenvalue of the y time simplex S_y^T is +1 for all single-particle states. This introduces three plane symmetries and allows us to restrict the numerical representation of individual wave functions to 1/8 of a full box [68]. In addition, the single-particle states are chosen to have good isospin projection (i.e. they are either pure proton or neutron states).

Mean-field states with different deformation are obtained by adding constraints on q_1 and q_2 as defined in Eq. (1) in the variation. The constrained HFB equations are solved by using the "two-basis method" described in Ref. [48], which delivers the HFB states $|q\rangle$ through quite a small number of single-particle states represented in coordinate space in the so-called Hartree-Fock (HF) basis that diagonalizes the single-particle Hamiltonian and the corresponding U and V matrices that establish the general Bogoliubov transformation [5,7,18] from the HF basis to the quasiparticle basis that diagonalizes the

quasiparticle Hamiltonian. This procedure permits us to limit the numerical representation to all single-particle levels below the Fermi energy and to a small number of levels above. As done in our earlier configuration-mixing calculations, we add the Lipkin-Nogami (LN) prescription to the HFB equations to enforce pairing correlations in all mean-field states. Using states without pairing in a GCM calculation introduces the danger of artificially decoupling many-body states with a different ratio of occupied single-particle states of positive and negative parity, which can lead to instabilities when solving the HWG equation (8).

The representation of the single-particle states on a coordinate space mesh has the clear advantage that its precision is fairly independent of the deformation when a sufficiently large box is chosen, and it only depends on the distance of discretization points. This is important for GCM calculations mixing states with very different deformation.

For the subsequent projection and mixing of HFB states with different shapes, it is advantageous to use the canonical single-particle bases of the mean-field states as a starting point. This simplifies the corresponding U and V matrices and allows for a safe cutoff of single-particle states with very small occupation v^2 that do not contribute to any of the kernels. For the identification of symmetries of the integrals over Euler angles, it also turns out to be advantageous to transform the single-particle basis to a basis of eigenstates of x signature $\hat{R}_x$.

B. Rotation of mean-field states

The rotation of the "left" state in coordinate space and the "right" state in gauge space, Eq. (18), can be performed either as rotations of the canonical single-particle states leaving the corresponding U and V matrices untouched or as rotations of the U and V matrices leaving the single-particle states untouched. For the coordinate space rotation, the latter is equivalent to the expansion of the rotated single-particle states in terms of the unrotated ones, which already at moderate deformation requires highly excited single-particle states above the Fermi energy, which are outside of the single-particle basis used to describe the unrotated state. Therefore, the coordinate space rotation $\hat{R}(\alpha, \beta, \gamma)$ is performed as a rotation of the single-particle states on the mesh as described in Refs. [14,84], which, however, is the most time-consuming piece of the numerical calculations. In contrast, it is simpler and numerically more efficient to perform the gauge-space rotation as a transformation of the V matrices instead of the single-particle basis, which in the canonical basis boils down to the multiplication of a small antidiagonal matrix with a phase factor.

The rotation operator $\hat{R}(\alpha, \beta, \gamma)$ mixes single-particle states of both signatures, which requires one to extend the numerical representation of the single-particle wave functions from 1/8 to 1/2 of the full box, leaving only parity (and the isospin projection) as a good quantum number. The symmetries of the unrotated time-reversal invariant HFB states, however, permit the reduction of the integration intervals for Euler angles to $\alpha \in [0, \pi/2]$, $\beta \in [0, \pi/2]$, and $\gamma \in [0, \pi]$

(i.e., 1/16 of the full $8\pi^2$ integration volume for systems with integer spin).

C. Calculation of the kernels between rotated mean-field states

Rotating an HFB state in coordinate or gauge space gives back an HFB state; hence, the matrix elements between "left" and "right" states, Eq. (18), can be easily evaluated with the generalized Wick theorem [5,58]. The expressions given in Refs. [5,58] cannot be directly used, however. First, we have to transform the contractions between states in different quasiparticle bases to expressions for contraction between states in different canonical single-particle bases [20,22]. Second, our coordinate space representation has as a consequence that the single-particle bases that set up $|q\rangle$ and $|q'\rangle$ are not equivalent, a difficulty that is amplified further by rotation of one of the states. This difficulty can be overcome by eliminating the contribution to the kernels coming from single-particle states that are occupied in one of the bases but not in the other [20,22,34,55].[2]

Only diagonal kernels and half of the off-diagonal ones have to be calculated; the other half of the off-diagonal kernels can be constructed by using symmetries of the kernels.

D. Particle-number projection and the phase of the overlap

The integrals over the gauge angles for projection on proton and neutron number are discretized with the Fomenko prescription [85], which is equivalent to a trapezoidal rule. By using the number parity of the mean-field states, the integration intervals can be reduced to $\phi \in [0, \pi]$ for protons and neutrons. Additionally, a symmetry connects the basic contractions and overlap in the interval $[0, \pi/2]$ with those in $[\pi/2, \pi]$, which, however, cannot be used to reduce the integration intervals for the reasons outlined in the Appendix of Ref. [22].

With the symmetries of the HFB states chosen here, the overlap of two HFB states with different deformation, where one is additionally rotated in coordinate space, remains real. As soon as one of the two HFB states is additionally rotated in gauge space, however, the overlap in general becomes complex. Its modulus is determined by the Onishi formula [5,19]. Its phase, a rapidly varying oscillatory function of the gauge angle of particle-number projection, has to be determined from continuity arguments. Its value is zero for the overlap between non-gauge-space-rotated states and is followed during the gauge-space rotation by performing a second-order Taylor expansion. To this end, the overlap and its derivatives are also determined at a small number of gauge angles between the integration points for the gauge-space integration, separately for protons and neutrons.

---

[2]The expressions for the matrices defining the basic contractions and the overlap given in Refs. [20,22,34] contain a systematical typographical error: All $(\mathcal{R}^{\dagger})^{-1}$ should be replaced by $(\mathcal{R}^{T})^{-1}$, which does not have any consequences for these papers as the matrix $\mathcal{R}$ is real with the symmetries chosen there.

[1] M. Bender, P.-H. Heenen, and P.-G. Reinhard, Rev. Mod. Phys. **75**, 121 (2003).

[2] S. Åberg, H. Flocard, and W. Nazarewicz, Annu. Rev. Nucl. Part. Sci. **40**, 439 (1990).

[3] W. Nazarewicz, Prog. Part. Nucl. Phys. **28**, 307 (1992); Nucl. Phys. **A574**, 27c (1994).

[4] S. Frauendorf, Rev. Mod. Phys. **73**, 463 (2001).

[5] P. Ring and P. Schuck, *The Nuclear Many-Body Problem* (Springer Verlag, New York, Heidelberg, Berlin, 1980).

[6] C. Y. Wong, Phys. Rep. **15**, 283 (1975).

[7] J.-P. Blaizot and G. Ripka, *Quantum Theory of Finite Systems* (MIT Press, Cambridge, Massachusetts, and London, England, 1985).

[8] B. Giraud and P. U. Sauer, Phys. Lett. **B30**, 218 (1969).

[9] F. Grümmer, K. W. Schmid, and A. Faessler, Z. Phys. A **300**, 77 (1981).

[10] K. Hara, A. Hayashi, and P. Ring, Nucl. Phys. **A385**, 14 (1982).

[11] A. Hayashi, K. Hara, and P. Ring, Phys. Rev. Lett. **53**, 337 (1984).

[12] E. Wüst, A. Ansari, and U. Mosel, Nucl. Phys. **A435**, 477 (1985).

[13] K. Enami, K. Tanabe, and N. Yoshinaga, Phys. Rev. C **59**, 135 (1999).

[14] D. Baye and P.-H. Heenen, Phys. Rev. C **29**, 1056 (1984).

[15] H. Zdunczuk, W. Satuła, J. Dobaczewski, and M. Kosmulski, Phys. Rev. C **76**, 044304 (2007).

[16] A. Kamlah, Z. Phys. **216**, 52 (1968).

[17] B. Beck, H. J. Mang, and P. Ring, Z. Phys. **231**, 26 (1970).

[18] H. J. Mang, Phys. Rep. **18**, 325 (1975).

[19] N. Onishi and S. Yoshida, Nucl. Phys. **80**, 367 (1966).

[20] P. Bonche, J. Dobaczewski, H. Flocard, P.-H. Heenen, and J. Meyer, Nucl. Phys. **A510**, 466 (1990).

[21] P. Bonche, J. Dobaczewski, H. Flocard, and P.-H. Heenen, Nucl. Phys. **A530**, 149 (1991).

[22] P.-H. Heenen, P. Bonche, J. Dobaczewski, and H. Flocard, Nucl. Phys. **A561**, 367 (1993).

[23] P. Bonche, S. J. Krieger, M. S. Weiss, J. Dobaczewski, H. Flocard, and P.-H. Heenen, Phys. Rev. Lett. **66**, 876 (1991).

[24] J. Skalski, P.-H. Heenen, P. Bonche, H. Flocard, and J. Meyer, Nucl. Phys. **A551**, 109 (1993).

[25] K. Zberecki, P. Magierski, P.-H. Heenen, and N. Schunck, Phys. Rev. C **74**, 051302(R) (2006).

[26] J. Skalski, P.-H. Heenen, P. Bonche, Nucl. Phys. **A559**, 221 (1993).

[27] J. Meyer, P. Bonche, M. S. Weiss, J. Dobaczewski, H. Flocard, and P.-H. Heenen, Nucl. Phys. **A588**, 597 (1995).

[28] J. Meyer, P. Bonche, J. Dobaczewski, H. Flocard, and P.-H. Heenen, Nucl. Phys. **A533**, 307 (1991).

[29] P.-H. Heenen, A. Valor, M. Bender, P. Bonche, and H. Flocard, Eur. Phys. J. A **11**, 393 (2001).

[30] M. Bender and T. Duguet, Int. J. Mod. Phys. E **16**, 222 (2007).

[31] K. Burzyski and J. Dobaczewski, Phys. Rev. C **51**, 1825 (1995).

[32] K. Enami, K. Tanabe, and N. Yoshinaga, Phys. Rev. C **63**, 044322 (2001).

[33] K. Enami, K. Tanabe, and N. Yoshinaga, Phys. Rev. C **65**, 064308 (2002).

[34] A. Valor, P.-H. Heenen, and P. Bonche, Nucl. Phys. **A671**, 145 (2000).

[35] M. Bender, H. Flocard, and P.-H. Heenen, Phys. Rev. C **68**, 044321 (2003).

[36] M. Bender, P. Bonche, T. Duguet, and P.-H. Heenen, Phys. Rev. C **69**, 064303 (2004).

[37] R. R. Rodríguez-Guzmán, J. L. Egido, and L. M. Robledo, Phys. Rev. C **62**, 054319 (2000).

[38] R. R. Rodríguez-Guzmán, J. L. Egido, and L. M. Robledo, Nucl. Phys. **A709**, 201 (2002).

[39] J. L. Egido and L. M. Robledo, in *Extended Density Functionals in Nuclear Physics*, edited by G. A. Lalazissis, P. Ring, and D. Vretenar, Lecture Notes in Physics **641** (Springer, Berlin, 2004), p. 269.

[40] T. Nikšić, D. Vretenar, and P. Ring, Phys. Rev. C **73**, 034308 (2006).

[41] T. Nikšić, D. Vretenar, and P. Ring, Phys. Rev. C **74**, 064309 (2006).

[42] K. W. Schmid and F. Grümmer, Rep. Prog. Phys. **50**, 731 (1987).

[43] K. W. Schmid, Prog. Part. Nucl. Phys. **52**, 565 (2004).

[44] P.-G. Reinhard and K. Goeke, Rep. Prog. Phys. **50**, 1 (1987).

[45] M. Girod, K. Kumar, B. Grammaticos, and P. Aguer, Phys. Rev. Lett. **41**, 1765 (1978).

[46] J. Libert, M. Girod, and J.-P. Delaroche, Phys. Rev. C **60**, 054301 (1999).

[47] L. Prochniak, P. Quentin, D. Samsœn, and J. Libert, Nucl. Phys. **A730**, 59 (2004).

[48] B. Gall, P. Bonche, J. Dobaczewski, H. Flocard, and P.-H. Heenen, Z. Phys. A **348**, 183 (1994).

[49] P. Bonche, H. Flocard, and P.-H. Heenen, Comput. Phys. Commun. **171**, 49 (2005).

[50] D. A. Varshalovich, A. N. Moskalev, and V. K. Khersonskii, *Quantum Theory of Angular Momentum* (World Scientific, Singapore, 1988).

[51] J. O. Corbett, Nucl. Phys. **A169**, 426 (1971).

[52] D. L. Hill and J. A. Wheeler, Phys. Rev. **89**, 1102 (1953).

[53] J. J. Griffin and J. A. Wheeler, Phys. Rev. **108**, 311 (1957).

[54] F. Dönau, J.-Y. Zhang, and L. L. Riedinger, Nucl. Phys. **A496**, 333 (1989).

[55] H. Flocard, thèse, Orsay, Sèrie A, **1543**, Université Paris Sud, 1975.

[56] D. Cline, Annu. Rev. Nucl. Part. Sci. **26**, 683 (1986).

[57] P.-G. Reinhard and C. Toepffer, Int. J. Mod. Phys. E **3**, 435 (1994).

[58] R. Balian and E. Brézin, Nuovo Cimento B **64**, 37 (1969).

[59] L. M. Robledo, Int. J. Mod. Phys. E **16**, 337 (2007).

[60] M. Anguiano, J. L. Egido, and L. M. Robledo, Nucl. Phys. **A696**, 467 (2001).

[61] J. Dobaczewski, M. V. Stoitsov, W. Nazarewicz, P.-G. Reinhard, Phys. Rev. C **76**, 054315 (2007).

[62] D. Lacroix, T. Duguet, and M. Bender (in preparation).

[63] M. Bender, T. Duguet, and D. Lacroix (in preparation).

[64] T. Duguet, M. Bender, K. Bennaceur, D. Lacroix, and T. Lesinski (in preparation).

[65] E. Chabanat, P. Bonche, P. Haensel, J. Meyer, and R. Schaeffer, Nucl. Phys. **A635**, 231 (1998); Erratum-*ibid.* **A643**, 441 (1998).

[66] C. Rigollet, P. Bonche, H. Flocard, and P.-H. Heenen, Phys. Rev. C **59**, 3120 (1999).

[67] P. Bonche, H. Flocard, P.-H. Heenen, S. J. Krieger, and M. S. Weiss, Nucl. Phys. **A443**, 39 (1985)

[68] P. Bonche, H. Flocard, and P.-H. Heenen, Nucl. Phys. **A467**, 115 (1987).

[69] M. Girod and B. Grammaticos, Phys. Rev. C **27**, 2317 (1983).

[70] M. Bender, G. F. Bertsch, and P.-H. Heenen, Phys. Rev. Lett. **94**, 102503 (2005); Phys. Rev. C **73**, 034322 (2006).

[71] M. Girod and B. Grammaticos, Phys. Rev. Lett. **40**, 361 (1978).

[72] N. Redon, J. Meyer, M. Meyer, P. Quentin, P. Bonche, H. Flocard, and P. H. Heenen, Phys. Rev. C **38**, 550 (1988).

[73] P. Möller, R. Bengtsson, B. G. Carlsson, P. Olivius, and T. Ichikawa, Phys. Rev. Lett. **97**, 162502 (2006).

[74] L. Guo, J. A Maruhn, and P.-G. Reinhard, Phys. Rev. C **76**, 034317 (2007).

[75] Z. Szymanski, *Fast Nuclear Rotation* (Clarendon, Oxford, 1983).

[76] W. Satuła and R. A. Wyss, Rep. Prog. Phys. **68**, 131 (2005).

[77] H. R. Dalafi, Nucl. Phys. **A252**, 42 (1975).

[78] A. S. Davydov and G. F. Filippov, Nucl. Phys. **8**, 237 (1958).

[79] A. S. Davydov and V. S. Rostovsky, Nucl. Phys. **12**, 58 (1959).

[80] K. Hagino, G. F. Bertsch, and P.-G. Reinhard, Phys. Rev. C **68**, 024306 (2003).

[81] R. B. Firestone, Nucl. Data Sheets **108**, 2319 (2007).

[82] J. Dobaczewski, J. Dudek, S. G. Rohozinski, and T. R. Werner, Phys. Rev. C **62**, 014310 (2000).

[83] J. Dobaczewski, J. Dudek, S. G. Rohozinski, and T. R. Werner, Phys. Rev. C **62**, 014311 (2000).

[84] D. Baye and P.-H. Heenen, J. Phys. A **19**, 2041 (1986).

[85] V. N. Fomenko, J. Phys. A **3**, 8 (1970).